https://doi.org/10.5194/egusphere-2026-2418
Preprint. Discussion started: 12 May 2026

Improved Dating of Landslides in Zimbabwe by Combining Satellite Multispectral and Synthetic Aperture Radar Observations

Joanna Noyes[1], Steven Palmer[1], Georgina Bennett[1], Seshagirirao Kolusu[2], and Caroline Bain[2]

[1]Department of Geography, Faculty of Environment, Science and Economy, University of Exeter, EX4 4PY
[2]UK Met Office, Fitzroy Road, Exeter, EX1 3PB

Correspondence: Joanna Noyes (jn511@exeter.ac.uk)

Abstract. Accurate dating of landslides is essential for understanding triggering mechanisms and improving hazard analysis, yet many inventories lack precise event timing. This study presents a two-step methodology for retrospectively dating landslides using multi-sensor satellite data and automated change-point detection implemented with the Ruptures Python package. In Step 1, extended time series of Sentinel-2 optical NDVI and the Bare Soil Index are analysed to estimate the approximate dates of landslides. Step 2 refines these estimates using Sentinel-1 SAR VV backscatter data within a six-month window (±90 days) centred on the results from Step 1. The approach is tested using a landslide inventory from Zimbabwe associated with Storm Idai in March 2019. Using the results from Step 2, 52.8% of the dataset is dated, with 84.6% accuracy (events correctly dated during the triggering storm event) and an average precision of 12.8 days (the dates between which the event occurred). The results demonstrate that combining optical and SAR satellite observations with automated change-point detection provides an effective method for retroactively dating landslides. This approach enables inventories to be dated with minimal prior knowledge of event timing or geometry, while avoiding the need for large datasets and high-performance computing resources. The code is made available in Google Earth Engine, allowing for wide application.

1 Introduction

Landslides are a global hazard, and in many cases result in significant damage, loss of life and economic costs (Froude and Petley, 2018; Petley, 2012). Haque et al. (2019) shows that between 1994-2014, an average of 8,877 people were killed by landslides each year. Precise dating of landslides is essential for determining their triggering conditions such as accumulation rates and antecedent rainfall, which is required for developing effective landslide early warning systems (Segoni et al., 2018; Baum and Godt, 2009). However, precise dating of landslides is limited or absent in many existing inventories, including collated inventories such as the Geological Survey of India (GSI) landslide inventory, NASA Cooperative Open Online Landslide Repository, or Global Landslide Catalog (GLC) (Geological Survey of India, 2024; Juang et al., 2019; Kirschbaum et al., 2009).

Larger landslides that impact communities and/or infrastructure and are therefore reported by media outlets can be effectively dated via news articles (Pennington et al., 2022), as demonstrated by the International Disaster Database (EM-DAT) or the global fatal landslide database (Delforge et al., 2025; Froude and Petley, 2018; Guzzetti et al., 2012). However, smaller and/or

https://doi.org/10.5194/egusphere-2026-2418
Preprint. Discussion started: 12 May 2026

remote landslides resulting in minimal human impacts are missed. Satellite data, typically multispectral observations, have been widely used to map and assess landslide hazards (Jaafari, 2024) but often lacks the temporal resolution to determine triggering conditions accurately (Yuniawan et al., 2022; Endo, 1969). Analysing large-scale weather patterns ideally requires daily sampling, with rainfall accumulations benefiting from hourly observations. However, due to the existence of cloud cover, many satellite based detection methods utilise brightest pixel averages or larger time windows to reduce the impact of cloud cover on their results (Milledge et al., 2022), and can result in monthly to yearly accuracy. While many attempts have been made to develop national inventories of past landslide events, there is a lack of consistency about the information that is recorded, and the dating is typically either missing entirely, or insufficiently precise to determine the antecedent conditions.

Table 1 summarises the studies that attempt to use satellite imagery to date landslides using a priori locations, but many are limited to relatively small datasets (<100 landslides). A common requirement across many approaches is the availability of landslide geometries (polygons), which are used to extract satellite signals from the affected areas. However, some inventories record only point locations rather than polygon geometries (Bostjančić et al., 2025; British Geological Survey, 2023). In addition, some approaches utilise more complex raw SAR data which require the download and processing of large satellite datasets. This can limit reproducibility and accessibility for researchers without specialised computing resources. Therefore, a method that requires minimal landslide information would allow a much larger number of existing inventories to be dated.

Table 1. Summary of selected landslide dating studies. Asterisks (*) indicate studies with satellite data records longer than those used in this study. GEE refers to Google Earth Engine. While all studies listed include landslide dating components, some address additional objectives therefore, differences in study goals should be considered when comparing performance metrics.

Study	Data Source	Data Type	Landslide Data	Geometry Input	Satellite Data Length	Resolution	Accuracy	precision
Burrows et al. (2022)	Sentinel-1	SAR	1000+ landslides	NA	6 months	20mx22m (60mx66m)	20-30% of data dated with an accuracy of 80%	12 days
Deijns et al. (2022)	Sentinel-1	SAR	2500 landslides	Geometries	January 2016 - January 2021	15mx15m (processed)	NA	1-47 days
Fu et al. (2023)	Landsat	multispectral	66 landslides	Geometries	1985-2017*	30mx30m	52% dated within 1 year of event	NA
Fu et al. (2024)	Sentinel-1 and 2	multispectral and SAR (GEE)	60 landslides	Geometries	Varied	10mx10m	NA	23 days average
Wang et al. (2024)	Sentinel-1	SAR (GEE)	7 landslides	Geometries	Varied (3-7 years)	10mx10m	NA	6-12 days
Burrows et al. (2025)	Sentinel-1	SAR	10,000	NA	3 months	20mx22m (60mx66m)	NA	NA
Barbera et al. (2025)	Sentinel-1 and 2	Multispectral and SAR (GEE)	46 landslides	Geometries	2018-2024	10mx10m	98% of events in vegetated areas encompassing 10+ Sentinel-2 pixels	3-12 days

This study will explore a simpler and more accessible method to retrospectively date landslides through the use of the Ruptures Python package (Truong et al., 2020). The proposed method requires only landslide point locations and freely available satellite data and is implemented using tools available through Google Earth Engine and Google Colab. This approach would expand the number of available datasets that can be dated, allowing for more pre-existing datasets to be utilised in triggering studies. Therefore, this study aims to create a method that:

https://doi.org/10.5194/egusphere-2026-2418
Preprint. Discussion started: 12 May 2026

- Can date landslides using remote sensing data
- Is readily available through Google Earth Engine and Google Colab
- Requires only landslide point information, allowing for more existing inventories to be dated using this method
- Has no a priori knowledge of landslide timings, utilising the whole Sentinel-1 time series (2015-present).

2 Data

2.1 Landslide data

This study utilises landslide data from Emberson et al. (2022), consisting of 1,319 individual slope failures within eastern Zimbabwe (Fig. 1). This was chosen to allow for direct comparisons with Burrows et al. (2022), as well as providing a large, well dated inventory for the accuracy of our new method to be assessed. Storm Idai, equivalent to a category 3 tropical cyclone (TC) at its peak, formed on the 4th March off the coast of Mozambique. Storm Idai first travelled east towards Madagascar, and then swung west-southwest back towards Mozambique, making landfall near Beira, Mozambique on 14th March as a category 2 TC . As Storm Idai continued to travel west, it further decreased in intensity to a tropical depression prior to crossing into Zimbabwe, before dissipating on 21 March just south of Harare, Zimbabwe. Figure 1b shows this path, with minimal rainfall over the region of interest before the 15 March 2019, and quickly falling by the 18 March. This supports the claims in Emberson et al. (2022) that the window of interest for these landslides spans from 15 March to between 20 and 24 March, with chosen end dates arising from the available satellite images used to date the original inventory. This report uses the range of the 15-20 March to classify whether an event has been correctly dated.

The landslide dataset is used here due to its prior application in Burrows et al. (2022), enabling direct comparison with their SAR-based dating approach. Although the original inventory contains polygon geometries, for this study each landslide was reduced to a point at the centroid of its polygon. Centroids were computed programmatically in Google Colab using the geometry centroid function applied to the original shapefile. This choice enables assessment of landslide dating performance when only minimal spatial information is available.

2.2 Satellite data

For this project, Sentinel-1 and Sentinel-2 data is used. Sentinel-2 red, blue, near-infrared (NIR) and short-wave infrared (SWIR) bands were utilised. Cloud masking was performed using the S2Cloudless cloud probability layer, which provides a per-pixel probability of cloud cover; pixels with cloud probabilities >40% were masked, offering improved accuracy over the default QA60 or Harmonized cloud/snow masks. Time series prior to 2020 were compiled from the standard Sentinel-2 collection, whereas post-2020 data used the Harmonized collection.

We use Sentinel-1 C-band VV (vertical-vertical backscatter) polarised Synthetic Aperture Radar (SAR) data. VH backscatter was also considered, but due to the improvement in the detection seen in VV over VH, VV was chosen for this method (visible

https://doi.org/10.5194/egusphere-2026-2418
Preprint. Discussion started: 12 May 2026

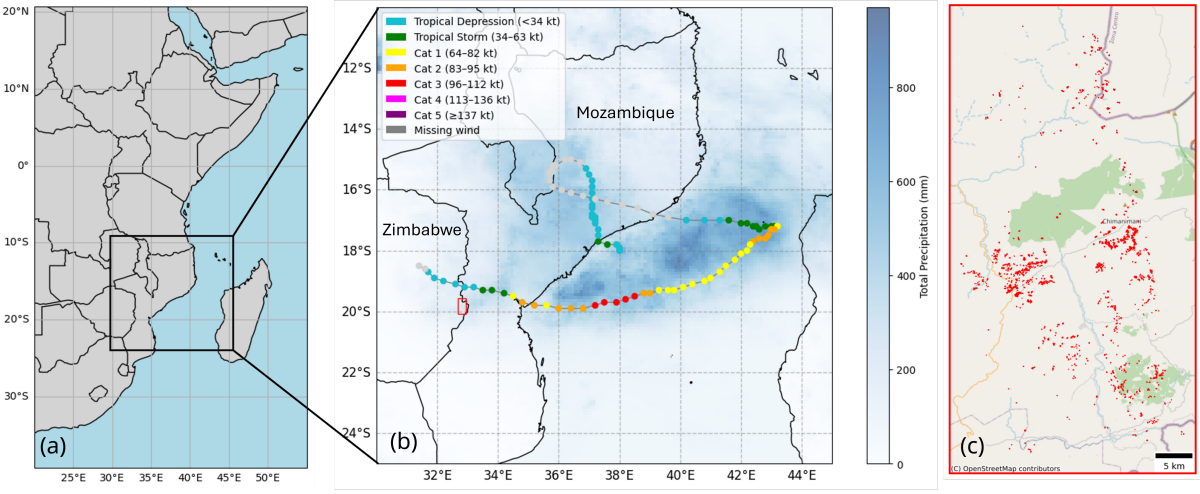

Figure 1. Figure showing a) the Area of Interest (AOI) for the landslides inventory from Emberson et al. (2022), b) the cyclone track, rainfall accumulation from the 4-21 March, and the wind speeds (from IBTRaCS (Knapp et al., 2010)) and c) the landslide inventory (Basemap in c): ©OpenStreetMap contributors).

in Fig. 7). Utilising both satellites aims to reduce the effective revisit time and improve the potential temporal resolution of the results of this project. Table A1 summarises the effective, best case scenario temporal resolution of Sentinel-1 and Sentinel-2 over the period 2014–present.

3 Method development and workflow design

Figure 2 shows the method flow in this study, and how dates are determined using both multispectral and SAR data. This workflow consists of two sequential steps. Step 1: using multispectral data from Sentinel-2 to determine a date for the event, and Step 2: refining that date using Sentinel-1 SAR data. The workflow was implemented using Google Earth Engine (GEE) and a connected Google Colab Jupyter Notebook environment, enabling scalable, cloud-based processing of planetary-scale satellite data. The method is openly available and can be reproduced by users with standard GEE and Colab access.

This study also utilises Ruptures Python code to assess the changes in the multispectral and SAR time series. Ruptures is a Python library used for offline change point detection which allows pattern changes in time series to be determined (Truong et al., 2020). Throughout this method, a combination of the squared euclidean distance (L2, the changes in mean) and the absolute distance (L1, the changes in median) are used to detect the changes that are expected from landslide activity. Ruptures also allows the strictness of the method to be altered, using a penalty. This means that higher penalties (p = 9) are less likely to return change points, whilst lower penalties (p = 0.5) are likely to return multiple per time series. It is important to note landslides detected using this method are disadvantaged when events occur earlier in the time series. This method compares average variables like the mean before and after the event. Time series that are able to recover, and experience the background

https://doi.org/10.5194/egusphere-2026-2418
Preprint. Discussion started: 12 May 2026

vegetation cycle for longer periods after the event, will see reduced contrast between the pre and post event mean. As this difference decreases, detection using this method becomes more difficult.

3.1 Step 1: Sentinel-2 multispectral time series dating

Due to the assumption that no information is known about the timing of these events, Step 1 utilises multispectral data. For the example discussed in this report, this ranges from 2015 to the end of 2023. This Step utilises the original Sentinel-2 image collection between 2015 and 2019, and then the updated harmonised collection after 2019 (Claverie et al., 2018; Drusch et al., 2012). Figure 3A shows the Normalised Difference Vegetation Index (NDVI) time series for the first listed landslide in the dataset. The following figures depict NDVI time series only, but both NDVI and BSI are used within the code provided.

3.1.1 Multispectral data set-up

NDVI, which measures the relative greenness of a pixel, is expected to show a sharp drop when a landslide occurs, due to the exposure of bare Earth following a slope failure. In vegetated areas, NDVI (range from -1 to +1) values are typically around 0.7, before falling to approximately 0.1 after a landslide, as shown in Table 2. Similarly, the Bare Soil Index (BSI), which ranges from –1 to +1, with vegetated regions estimated from data to be around -0.5, increasing to around 0.

$$\mathrm{NDVI} = \frac{\mathrm{NIR} - \mathrm{RED}}{\mathrm{NIR} + \mathrm{RED}} \tag{1}$$

$$\mathrm{BSI} = \frac{(\mathrm{SWIR} + \mathrm{RED}) - (\mathrm{NIR} + \mathrm{BLUE})}{(\mathrm{SWIR} + \mathrm{RED}) + (\mathrm{NIR} + \mathrm{BLUE})} \tag{2}$$

Table 2. Expected NDVI ranges from different surfaces (Korchagina et al., 2020) and the approximate BSI values obtained from a Sentinel-2 image (16 June 2024) over Eastern Zimbabwe/Western Mozambique. BSI values are not representative of global BSI ranges but are directly comparable within this image.

Type	NDVI	Approximate BSI
Dense vegetation	0.7 to 1.0	-0.6 to -0.4
Sparse vegetation	0.2 to 0.5	-0.05 to -0.07
Soil	0.025 to 0.2	-0.12 to 0.03
Cloud	0	0.2 to 0.6
Snow/Ice/Dust/Rock	-0.1 to 0.1	-0.16 to -0.05
Water	-0.42 to -0.32	None Detected

This method relies on the removal of vegetation by landslides and exposure of a landslide scar, often visible from satellites in vegetated regions and commonly used to map landslides (Milledge et al., 2022; Wen and Teo, 2022; Zhong et al., 2019). During a landslide, NDVI captures the decrease in vegetation cover, while BSI captures the increase in exposed soil. Although

https://doi.org/10.5194/egusphere-2026-2418
Preprint. Discussion started: 12 May 2026

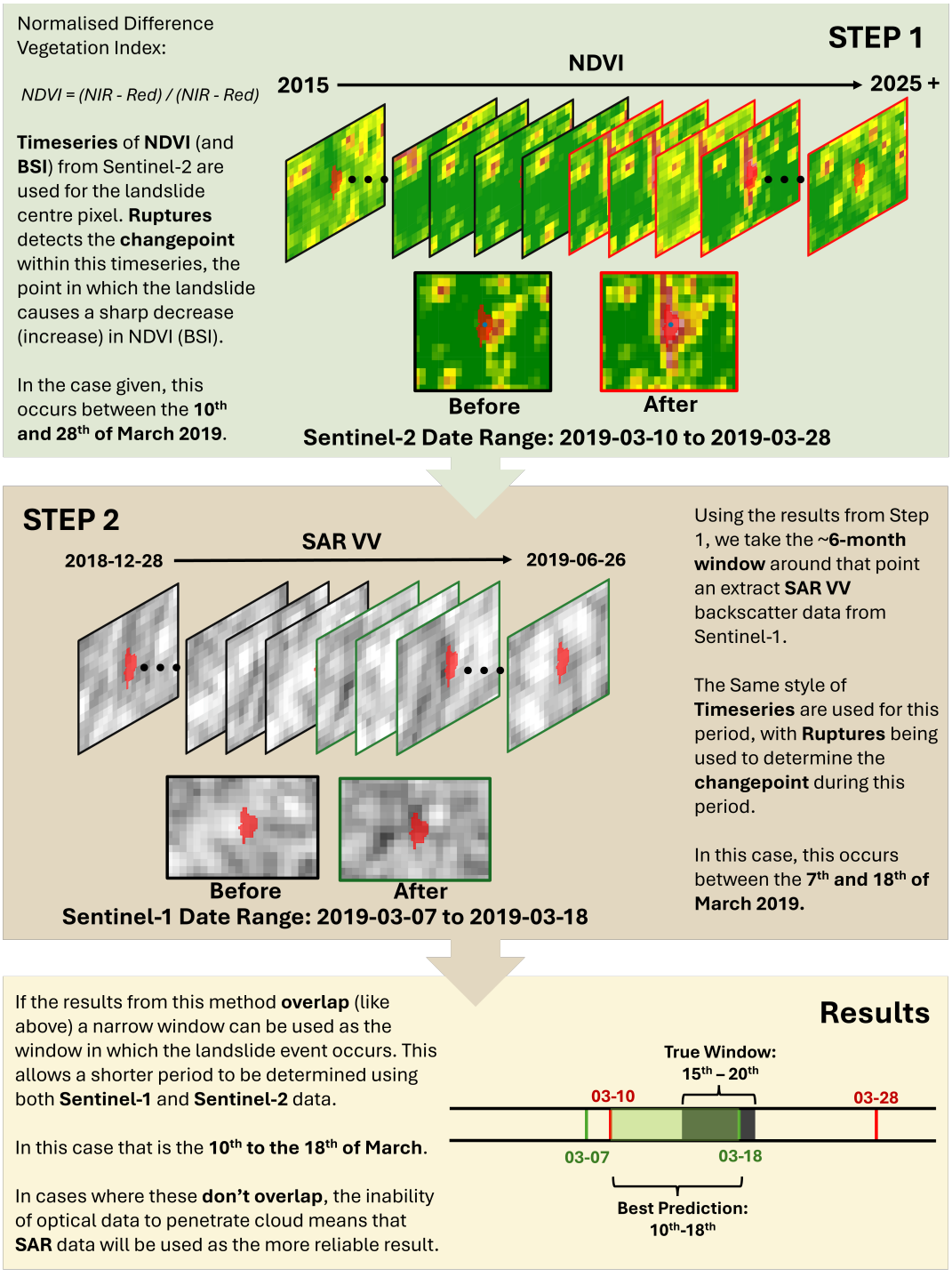

Figure 2. Schematic of the Flow of the method

https://doi.org/10.5194/egusphere-2026-2418
Preprint. Discussion started: 12 May 2026

these indices are often inversely related, they are derived from different spectral bands, and bare soil and vegetation are not the only land-cover types; hence, the indices are not always directly anti-correlated. Utilising more than one index allows for more observed spectral information to be utilised in the method (i.e. shortwave-infrared (SWIR), near-infrared (NIR), red and blue bands). This approach also provides an additional detection metric, strengthening results when both methods agree without significantly increasing computation time.

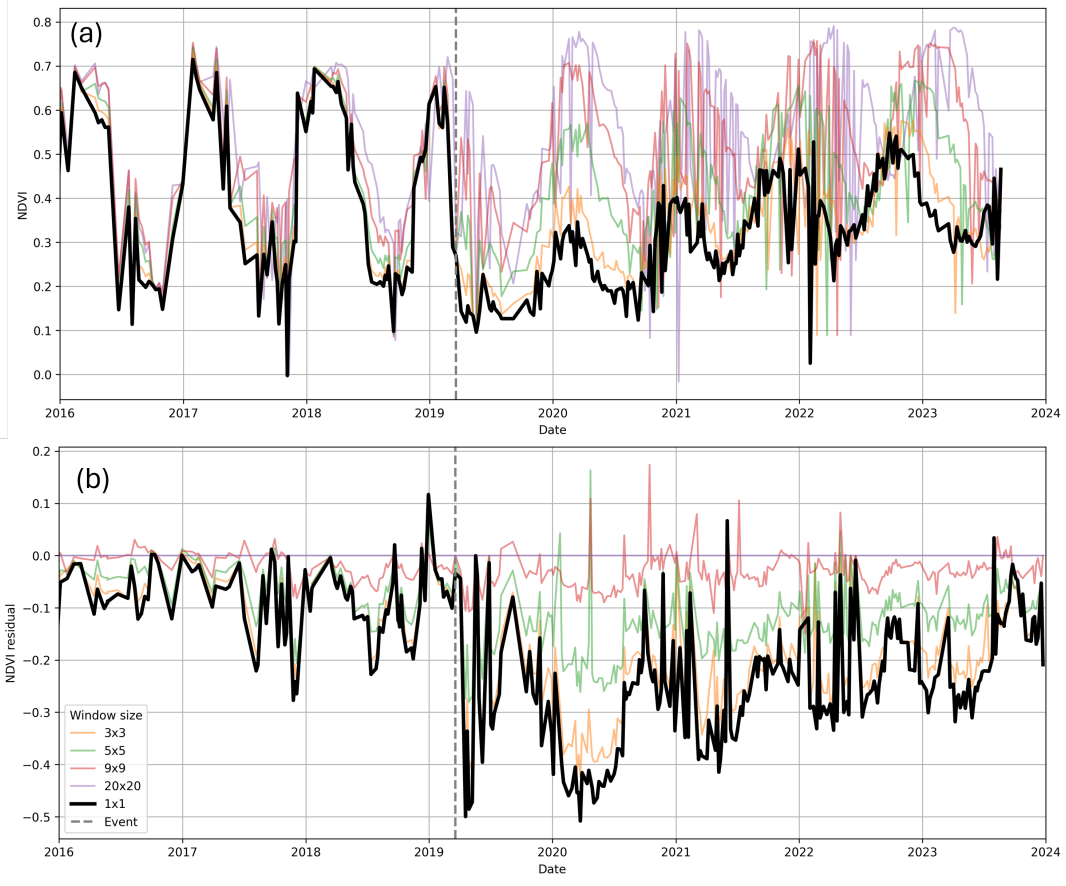

Figure 3. NDVI time series for a landslide within the Zimbabwe dataset showing the a) NDVI for a given point and b) the NDVI for that point minus the NVDI mean for the surrounding 100 m radius. Black shows the results for a single pixel 1x1 (10mx10m), orange = 3x3 pixels, green = 5x5 pixels, red = 9x9 pixels, and purple = 20x20 pixels (approximate 100 m radii results). The event is shown by the dashed line at 2019-03-15

Figure 3 shows the time series for a single 10 m by 10 m pixel centred on an individual landslide scar. Landslide areas typically follow a power-law size distribution, with many small failures and comparatively few large events (Malamud et al., 2004). Assessments of this specific dataset show that 77% of the landslides are smaller than 25 total pixels (2500m^2). Using larger areas of interest (AOIs) reduces the impact of random noise but also smooths and minimises the signal from the landslide

https://doi.org/10.5194/egusphere-2026-2418
Preprint. Discussion started: 12 May 2026

event. This is evident in Fig. 4, showing that larger regions of interest are quickly dominated by background vegetation, rather than the spectral signature of the landslide. Again, an AOI of 25 pixels has an area where around 50% is comprised of the landslide. These larger areas, if not geometry specific, are therefore at risk of smoothing landslide triggering, either missing or falsely labelling these collapses. This is supported by the larger AOI time series shown on Fig. 3A.

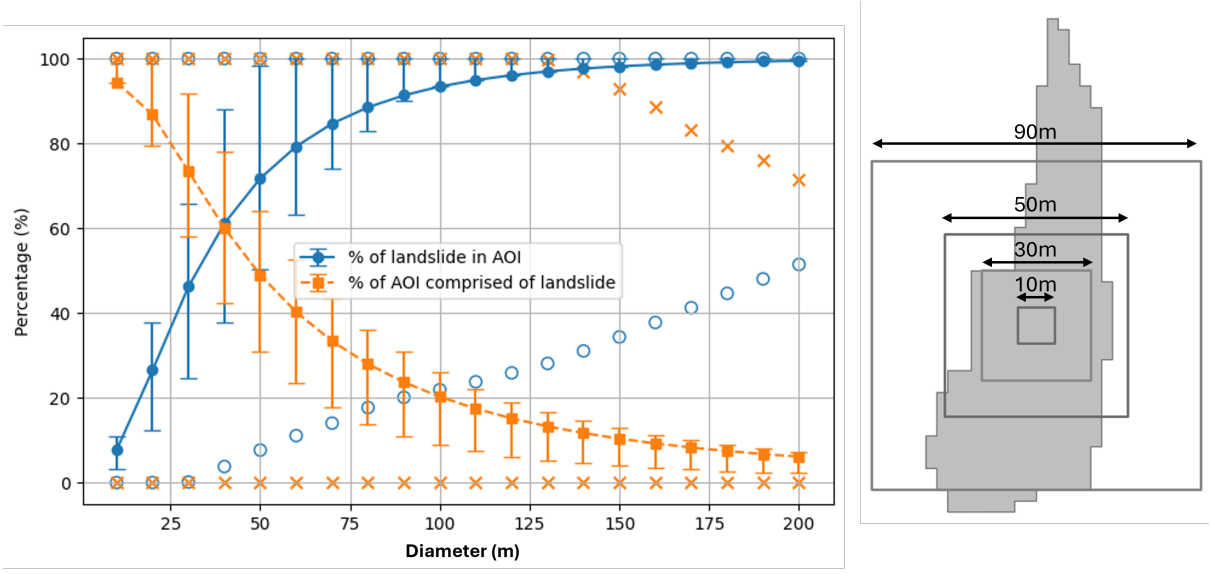

Figure 4. Percentage of the landslide within the AOI (blue) and the percentage of the AOI in the landslide (orange). Each buffer is represented by the mean, interquartile range (bar) and the minimum and maximum percent within the dataset for that point. The diagram to the right shows one landslide example, with the box for 1x1, 3x3, 5x5, and 9x9 drawn.

Absolute NDVI values at a single pixel (Fig. 3a) exhibit strong seasonal variation, with greening during the wet months and reduced vegetation during the dry season. Landslides cause abrupt drops in NDVI, but this signal can be masked by seasonal trends and local noise, making change-point detection with Ruptures challenging. To mitigate this, the NDVI residuals are computed relative to the surrounding region (100 m buffer), effectively removing local seasonality and systematic noise while highlighting abrupt changes due to landslides:

$$\Delta\text{NDVI} = \text{Point NDVI} - \text{Average of Surrounding NDVI}$$

Figure 3B shows the results from Fig. 3A minus the time series calculated for a buffer of 100 m. Calculating this residual removes the annual seasonality before the event, reducing the overall variation in NDVI prior to the landslide. The annual seasonal variations are still present in the post event time series, as the landslide location experiences little seasonal changes compared to the surrounding region. This results in an offset seasonal variability after the event, as seen in Fig. 3B. While this examples shows significant noise, using residual multispectral signals significantly improves change-point detection with

https://doi.org/10.5194/egusphere-2026-2418
Preprint. Discussion started: 12 May 2026

Ruptures, with the correct landslide date being identified with harsher restrictions of the change-point methods. Furthermore, Ruptures can list multiple change-points per each point examined. This method picks the first change-point that can be detected. Therefore, improving the variability in NDVI before the event (to the detriment of the noise after) is beneficial, as the first detected point determines the reported date.

It is important to note that this approach will be less effective for larger landslides, because the buffer will contain a larger ratio of landslide to background environment. However, Fig. 4 shows and average of less than 10% of this 100 m radius (200 m diameter) is comprised of the landslides, with most of the dataset falling between 0-10%. The residual NDVI picks up the date of the landslide more effectively than the NDVI for the pixel alone. Using the residual results is a slower method, as more pixels are being processed. However, as this is working with historical landslide data with no requirement to be updated in near-real-time , the quality of the results is more important than the computational speed.

3.1.2 Multispectral change point detection method

Stricter Ruptures methods, with higher penalties, return more reliable results as the requirements for detecting a change are higher. However, the strictest method, L2 penalty 9, only dates 3% of points, with Fig. 5 showing that of the first 150 points, L2 penalty 9 only dates 4 of them. To balance result reliability and quantity, a hierarchical selection process is implemented within Step 1 of the method. L2 penalty 9 returns the highest quality, and is used where available. For events not dated at this level, progressively less strict penalties are applied in descending order of assumed reliability. Figure 5 shows the accuracy of each method, with L2 penalty 9 returning a 75% accuracy, L2 penalty 5 a 69% percentage accuracy, and so on. The six largest percentages have been used in this method, with L2 penalty 0.5 dating 70% of the results, at a 48% accuracy. The hierarchical selection process applies the following Ruptures configurations in order of preference is shown in Eq.(3).

$$\text{Preference ranking: L2 penalty 9} > \text{L2 penalty 5} > \text{L1 penalty 9} > \text{L1 penalty 5} > \text{L2 penalty 1} > \text{L2 penalty 0.5} \quad (3)$$

For each landslide, the highest-ranking configuration that produces a valid change point is selected. This set of configurations spans a sufficient range of penalty values to balance robustness and coverage. Additional intermediate penalty values were not included, as lower penalties primarily increase the number of detections rather than improve result reliability. It is important to note that this is Step 1 (Fig. 2), and many incorrectly dated points are further filtered out later in the process.

This method allows landslide inventory to be batch processed, and returns a dataset comprised of: the coordinates, the detected date, the index used (NDVI, BSI, both), the Ruptures configuration (method and penalty), the date before and after the event, and whether the point is filtered for physically plausible changes in NDVI/BSI. Step 2 results update the dates given to the new SAR based result, and the rest of the dataset remains the same. Additional statistical data such as mean and standard deviation for the whole time series as well as before and after the event is not provided in the end result, but is used to remove invalid points.

Multispectral data allows long time series (in this study 2015-present day) to be effectively analysed for landslide detection. This can be even longer in methods that utilise Landsat like Fu et al. (2023) where 1985 to 2017 was analysed. However, the

https://doi.org/10.5194/egusphere-2026-2418
Preprint. Discussion started: 12 May 2026

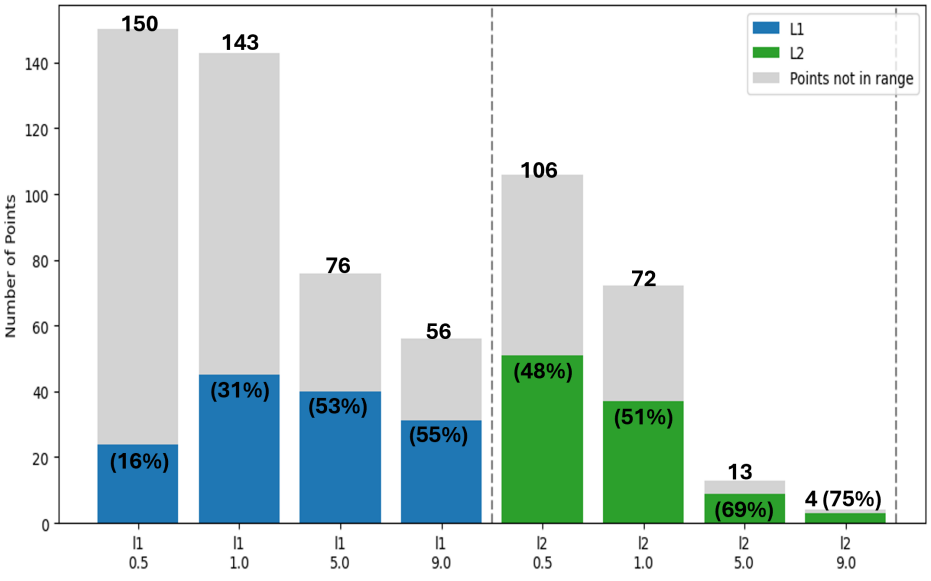

Figure 5. The number of points dated (grey) for each method, and the number of those dated correctly (spanning 15-20 March 2019) for Ruptures method L1 (blue) and L2 (green). This uses the established method for the first 150 indices in the dataset. This shows the total number of each penalty dated, and the percentage of that dated correctly.

main limitation of this method is the inability of multispectral data to penetrate cloud cover. This is particularly problematic in the case of rainfall-induced landslides where cloud cover is typically present at the time of the slope failure. Cloud pixels are removed, and therefore the derived time series has no observation for that date. Ruptures detect the first date where the trend of the time series has changed, and this method then also saves the previous pixel date. In cases where cloud removes data, the method will return the date of the first cloud-free observation after the landslide occurred, therefore biasing the recorded date (Singh et al., 2025; Fu et al., 2024). Additional steps are therefore needed to further improve the accuracy of these results.

3.2 Step 2: Sentinel-2 SAR time series dating

Incorporating SAR imagery provides two key advantages: (1) additional information to improve the results derived from Sentinel-2 data, and (2) an overlapping but distinct acquisition cycle that helps narrow the temporal window during which a landslide event is likely to have occurred. The acquisition frequencies of Sentinel-1 (SAR) and Sentinel-2 (multispectral) are summarised in Table 2.

3.2.1 SAR data set-up

As a leading aim of this project is to create a method fully contained within Google Earth Engine, the Sentinel-1 C-band synthetic aperture radar (SAR) VV backscatter amplitude data from descending passes were used. SAR VV backscatter is mostly sensitive to surface roughness and soil moisture, which can highlight changes in vegetation or surface texture (Burrows et al.,

https://doi.org/10.5194/egusphere-2026-2418
Preprint. Discussion started: 12 May 2026

2022). This data has been smoothed to reduce noise and improve change point detection. Unlike phase-based interferometry, which measures precise displacement, amplitude changes indicate abrupt alterations in radar scattering properties, which occur during landslides (Wang et al., 2024; Deijns et al., 2022; Burrows et al., 2022). Figure 6 shows that the long time series of SAR does not possess a continuous annual pattern like NDVI in Step 1 (Fig. 3a) and therefore the change that denotes the landslide event is lost within the noise of the longer time series. Using the same change detection approach as the multispectral Sentinel-2 data is therefore not suitable.

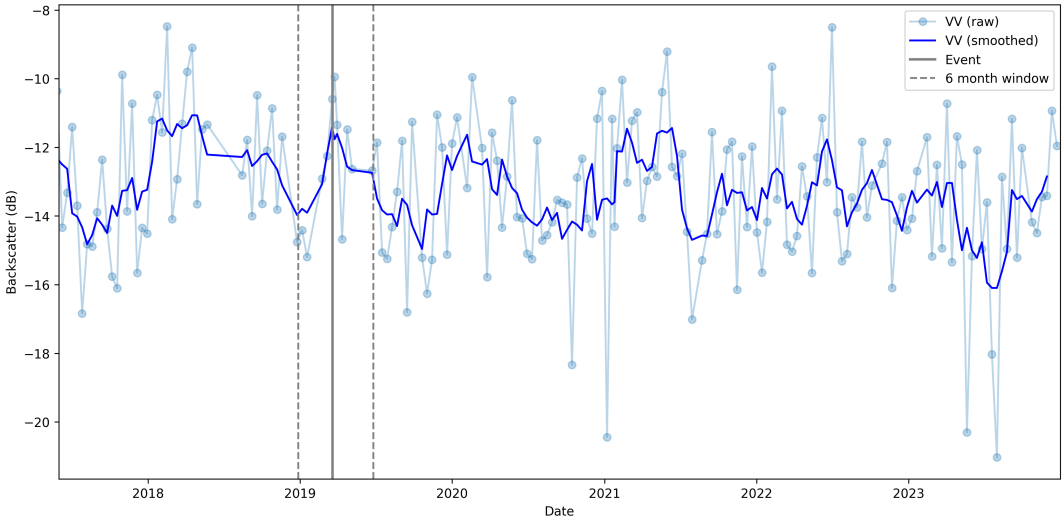

Figure 6. Complete Time series of VV SAR backscatter. This shows both the point values and the smoothed (3 consecutive point) time series. The landslide event is shown at 20 March 2019 (solid vertical line), with the ± 90 day window falling between the dashed lines.

Observing the period where the event occurs, a change is evident. But there is not a sustained change over time, unlike in the multispectral data. Therefore, a shorter time window is needed for Ruptures to accurately date this event. Figure 7 shows the distribution of landslides dated correctly after Step 2 using different windows of time, assuming Step 1 dated the events correctly. As the window increases, the number of points dated correctly increases to 100% at a window size of ± 80 days. However, as the window becomes larger, the likelihood of a false detection happening earlier increases, and the percentage falls back to zero. A window of ± 80-100 days results in 71% of the points being dated, 100% of which are dated correctly. Therefore, we utilise a window of ± 90 days. This reflects the periods utilised in Burrows et al. (2022).

3.2.2 SAR changepoint detection method

The SAR time series is significantly shorter than that of the multispectral data, and the change from the landslide is much smaller. Therefore, method L2 with a penalty of 1 has been used, rather than the hierarchical picking used in Step 1. These results are shown in Fig. 7, highlighting that L2 penalty 1 results in the 71% of results being dated, 100% effectively in that sample.

https://doi.org/10.5194/egusphere-2026-2418
Preprint. Discussion started: 12 May 2026

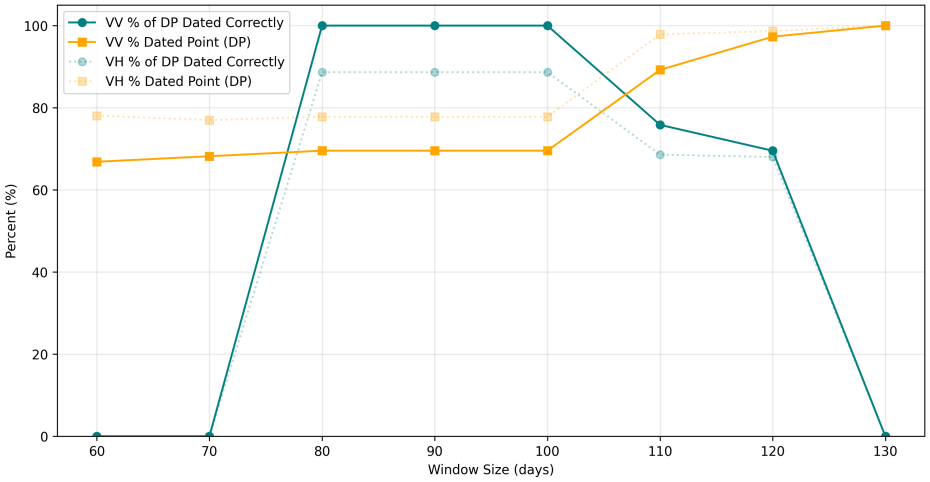

Figure 7. The percentage of points dated in comparison to the window size (teal) and the percentage of those dated landslides that are dated correctly (correctly dated = the image at the start and end of the detected change falling between 16-20 March 2019) (orange). The VV data is shown by the solid line, and the dotted line shows the VH data.

In the case where both the multispectral and SAR data agree, the window in which the event occurs can be reduced depending on the overlap in the data. In cases of discrepancy, the SAR dates are treated as the more reliable result. This is due to the cloud cover in Step 1 likely resulting in incomplete time series and offset dating within the multispectral data.

3.3 Post-processing

NDVI is expected to result in a drastic drop when a landslide occurs. Similarly, BSI shows a sharp increase after a landslide event. The method in this project utilises these sharp changes by determining dates which experience a change in mean (L2) or median (L1) between the index prior to the event in comparison to points after the event. However, this method does not discriminate between positive or negative mean changes. Based on established theory, only negative NDVI changes and positive BSI changes are physically plausible in the context of landslide detection. Figure A1 shows a section of results from this method in relation to the mean change polarity, which further supports the known theory that positive NDVI mean changes and negative BSI changes result in incorrect dating. In removing these points, they are also removed from Step 2 of this method. Therefore, this method ensures these points are removed, and not counted within the final results. This step removes very few correctly dated points but increases the proportion of points overlapping the 15–20 March 2019 window from 78.7% to 84.6% (discussed further in results).

https://doi.org/10.5194/egusphere-2026-2418
Preprint. Discussion started: 12 May 2026

4 Results

Using the combined multispectral and SAR workflow, 52.8% of the 1319 landslides were assigned a date in Step 2, of which 84.6% were correctly dated within the 15–20 March 2019 window. A landslide is considered **correctly dated** if the final estimated date window overlaps with the event window of 15-20 March 2019. Precision is described as the length of time (in days) between the satellite images that the landslide is detected between. Figure 8A shows a sample of the landslides dated in this study. Figure 8B shows the results that arise when combining the dates given by Step 1 and 2, where we see a decrease in precision (12.8 days to 11 days average) but a decrease in accuracy, with only 68.5% of results being dated correctly. Therefore, within this method, the Step 2 results alone are used.

Table 3 shows the distribution of the results according to their overlap with March 2019 and the correct date window of the 15-20 March 2019. Table 4 shows the distribution of windows that the landslides fall within according to Step 2 of this method, and Step 1 and 2 combined. This table shows an improvement in the overall precision of the results but a decrease in the accuracy when the two steps are combined, due to the Step 1 dates that occur before the event. When combined, this results in landslides being dated before the event. Such points are shown in Fig. 8B.

Table 3. Summary of Results for Step 1, Step 2, and Overlap Analysis. Step 1 Total Points Dated includes points detected by NDVI only, BSI only, and both indices. Percentages represent the percentage of the total points dated during that step (bold).

Stage	Metric	Value
Step 1	Total Points	1319
	Points Dated (NDVI only)	*196*
	Points Dated (BSI only)	*42*
	Points Dated (both)	*725*
	Total Points Dated	**963**
	In March 2019	738 (76.6%)
	Overlapping 15–20 March 2019	385 (40.0%)
Step 2	No. available for Step 2	963
	Total Points Dated by Step 2	**696**
	In March 2019	607 (87.2%)
	Overlapping 15–20 March 2019	589 (84.6%)
Overlap	*Overlapping 15–20 March 2019*	*477 (68.5%)*

The results from this model have been evaluated to determine factors that influence the reliability and accuracy of the results. The descending SAR track is moving approximately south, with a right facing look direction. We would expect to see improved results on the easterly facing slopes due to stronger signals despite distortion (Woodhouse, 2017). Furthermore, steeper angles, particularly those facing away from the satellite, can be influenced by shadows. Figures 9 and A2 show the aspects and slope distributions of the landslides respectively. The results in this study utilise the descending signal only.

https://doi.org/10.5194/egusphere-2026-2418
Preprint. Discussion started: 12 May 2026

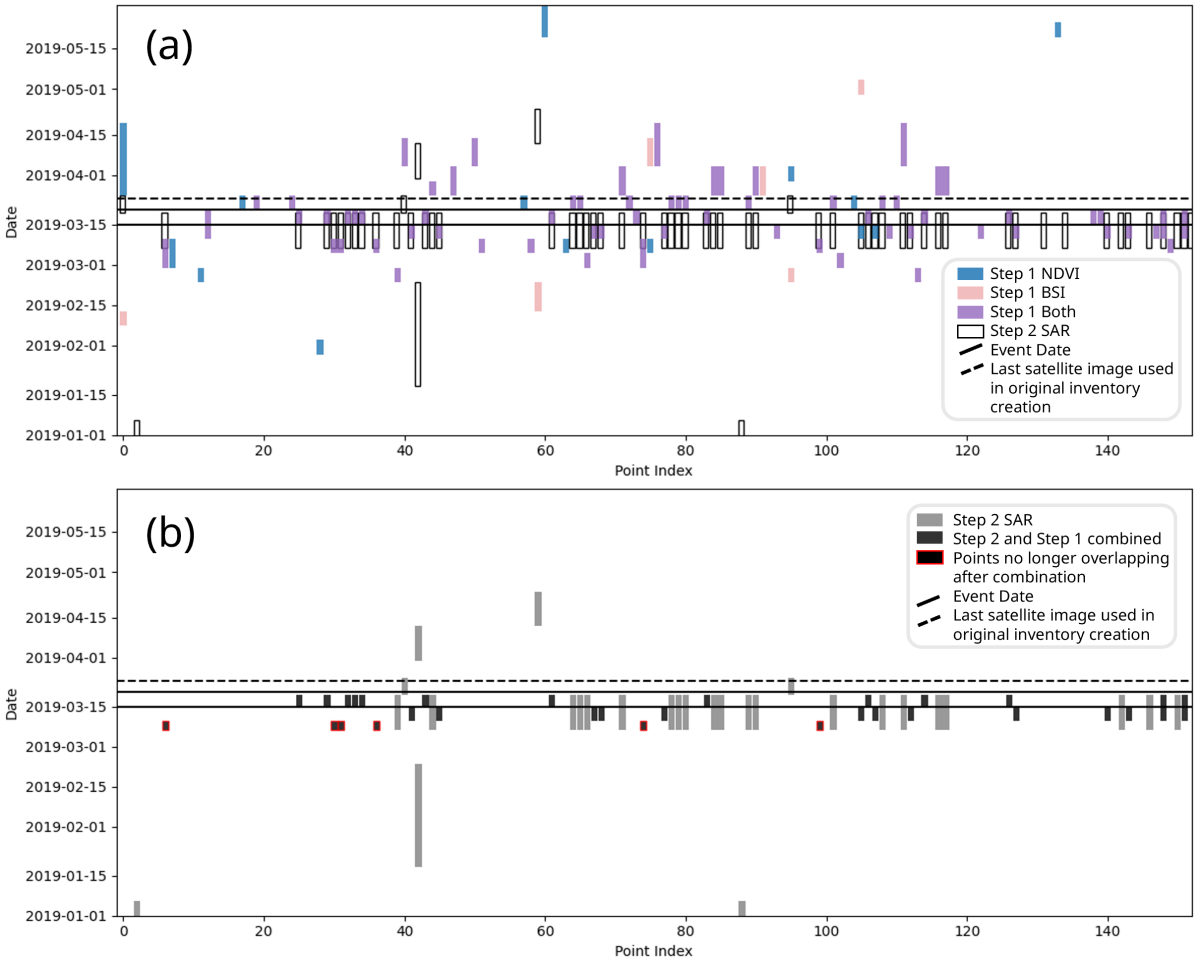

Figure 8. The first 150 landslides dated. Solid black lines represent the period Storm Idai impacted Zimbabwe (15-20 March 2019 according to Emberson et al. (2022)), with the dashed line representing the last image used to date the original landslide inventory (24 March 2019). a) Step 1 multispectral results (pink = BSI, blue = NDVI, purple = both) and Step 2 SAR results (black outline). b) shows the combined results of Step 1 and 2. Black boxes show where the SAR and multispectral results/dates (Step 1 and 2) overlap. When no overlap is present the SAR result has been listed (grey box). Red outlined boxes indicate points where Step 2 is correct, but Step 1 dating causes the combined result to be incorrect.

https://doi.org/10.5194/egusphere-2026-2418
Preprint. Discussion started: 12 May 2026

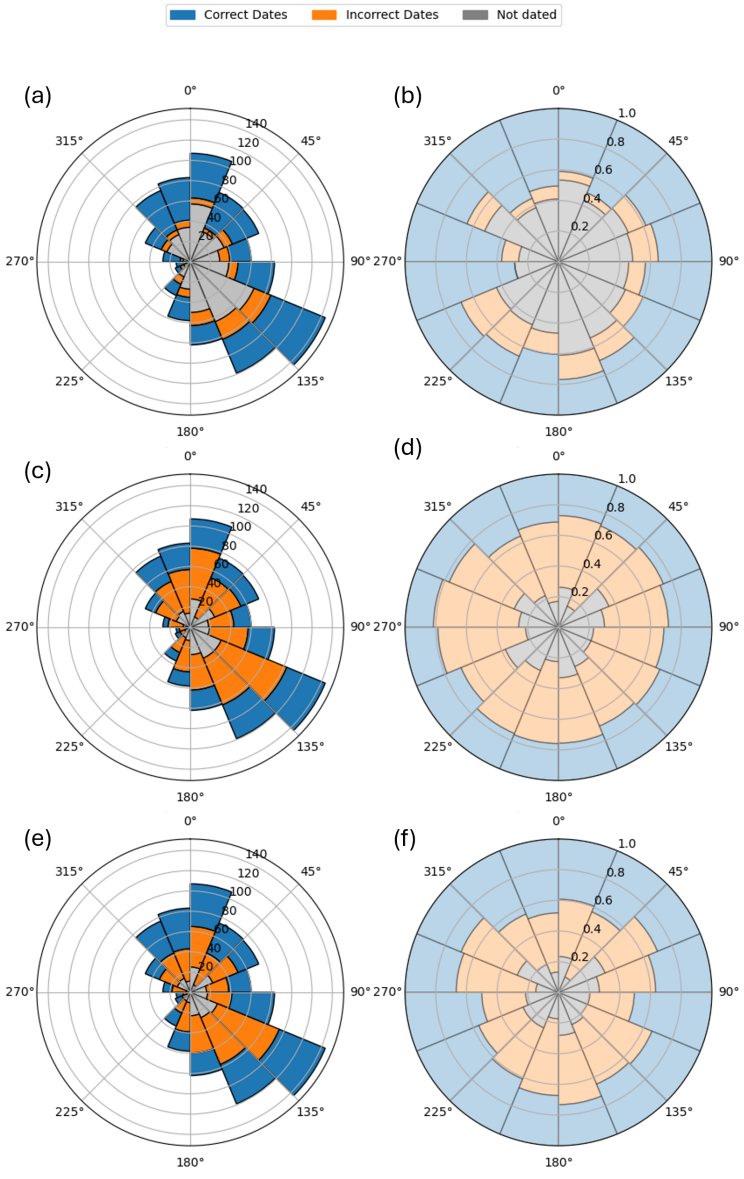

Figure 9. Distribution of correctly (blue), incorrectly (orange), and not dated (grey) landslides with respect to slope aspect derived from the SRTM 1 Arc-Second Global digital elevation model NASA JPL (2013). The results from the descending (a and b), ascending (c and d) and both (e and f) SAR data are shown. a), c), and e) show the absolute distributions in respect to aspect, whilst b), d) and f) show the normalised distribution across each aspect.

https://doi.org/10.5194/egusphere-2026-2418
Preprint. Discussion started: 12 May 2026

Table 4. The distribution of precision (date windows in days) from the results of Step 2 and the results from combining Step 1 and 2. Window periods include both the beginning and end date between which a landslide has been dated (e.g. one week is 8 days). The two rows labelled with worsened are the only rows where the accuracy of the results in Step 2 are reduced by combining them with Step 1. Of the 99 incorrect at a 4 day window, 97 are dated correctly in Step 2. For the 1 day window, 25 are dated correctly in Step 2, dropping to 9 in the combined data. For the range of 4 days: Step 1 mostly dates between 5-10 March 2019, and 28 February to 10 March 2019 (the results of which were shown in red on Fig. 8). [*This includes dates that have no overlap. As dates that do not overlap are saved as the Step 2 date].

Date Window (days)	**Step 2 Results (higher accuracy)**		**Combined Step 1 and 2 (better precision)**	
	Correct	Incorrect	Correct	Incorrect
1			9 (Worsened)	29 (Worsened)
2			0	1
4			0 (Worsened)	99 (Worsened)
5			34	1
6			30	4
7	24	2	24*	2*
9			2	2
10			77	0
11			0	1
13	565	94	301*	73*
16			0	4
21			0	1
25	0	1	0	1*
37	0	10	0	1*
TOTALS	589 (84.6%)	107 (15.4%)	477 (68.5%)	219 (31.5%)

5 Discussion

Using the method in this report, 696 of 1319 total landslides were dated, of which 589 (84.6%) of the Step 2 dates fall within the expected date range (15-20 March 2019) and 87.2% of the results fall within March 2019 (Table 3). These results align with those in Burrows et al. (2022), which saw accuracies of approximately 80%. Our method improves upon the number of points dated, increasing from 20–30% in previous studies to 52.8% in this study, highlighting the benefit of this Ruptures-based approach which utilises both multispectral and SAR observations. The results from this method improve upon the 52% seen in (Fu et al., 2023), and whilst it sees a lower accuracy than Barbera et al. (2025), a much larger sample size has been used. It is important to note that Burrows et al. (2022) additionally focuses on landslide detection and spatial delineation, whereas the present study is concerned solely with retrospective dating. These methods therefore serve complementary rather than directly competing purposes.

https://doi.org/10.5194/egusphere-2026-2418
Preprint. Discussion started: 12 May 2026

95.9% of the correctly dated results fall within a 13-day precision window, between 7-19 March 2019 (including both the beginning and last day), evident both from Table 4 and Fig. 8A. This is dependent on the satellite data available and is comparable to those in Burrows et al. (2022). Similar results are seen in Wang et al. (2024) and Barbera et al. (2025), with an improvement on the 23-day average seen in Fu et al. (2023) (Table 1). Table 4 shows the distribution of the results when combining outputs from Step 1 and 2. This shows that including SAR observations in step 2 leads to an improvement in the precision of the results, with some results being narrowed down to a single day. However, combined results see a decline in accuracy, from 589 to 477 (dropping accuracy down to 68.5%). This is the result of the 112 landslides that are dated correctly in Step 2, but not in Step 1, reducing the accuracy of the 1-day and 4-day window in the combined results. This is likely due to non-masked cloud cover decreasing the NDVI values, resulting in landslides being detected prematurely. The temporal precision and accuracy of Step 2 alone is 84.6% dated to an average of 12.8 days, while the combined show an accuracy of 68.5% dated to an average of 11 days. Due to the decrease in accuracy and relatively small improvement in precision, Step 2 alone provides the best results from this method.

Other studies explore much smaller numbers of landslides (7-66, Table 1) and therefore direct comparisons are hard to make between the results in this study and Barbera et al. (2025), Wang et al. (2024) and Fu et al. (2024). Furthermore, studies like Barbera et al. (2025), which use a similar multispectral and SAR method, only utilise their method for landslides encompassing at least ten 10 m by 10 m pixels that are well vegetated. Whilst small, such limitations are seen within many of the studies listed in Table 1, including Burrows et al. (2022). This is therefore a benefit of the method presented in this study, which does not see any bias against small size landslides, and does not require any knowledge of landslide geometry (Fig. A4). Due to this method only using one case study, the importance of vegetated slopes for the efficacy of this method requires further testing. Step 1 does require a decrease in vegetation for a shift in NDVI values to be detected, but the vegetation density threshold required for reliable dating of a landslide using this method is unknown.

Overall, this method benefits from the 2-stage process of integrating both Sentinel-2 multispectral and Sentinel-1 SAR data. The multispectral component of this method allows for a larger time window to be studied. Multispectral indices like NDVI are commonly used for dating landslides, due to the strong signal after a landslide event (Fig. 3) (Milledge et al., 2022; Zhong et al., 2019). Ruptures works by assuming a time series can be split into segments with different statistical properties (Truong et al., 2020), with L2 detecting mean shifts. Ruptures is therefore good at detecting rapid landslide changes, like those seen in this case study (Fig. 3). This allows for long time series to be quickly assessed for landslide activity. Of the 1319 points, 963 were dated within the time series of 2015 to 2024, 76.6% of which were dated within March of 2019. But it is evident from Fig. 8A that the Step 1 results are noisy, with only 40.0% of them being dated correctly. Again, this is expected, with multispectral data being affected by atmospheric conditions like cloud cover and lighting conditions. SAR data does not have this issue, as the microwave signal it utilises penetrates through cloud. The multispectral data (Step 1) of this method provides the 6-month window in which Step 2 is carried out using SAR. This method utilises the full Sentinel-2 time series (2015-present) whilst also using the improved accuracy of the SAR data, like Fu et al. (2024) and Barbera et al. (2025).

Satellite SAR sensors like Sentinel-1 make use of a side-looking acquisition geometry to enable images to be derived, which leads to some well-documented terrain-related artefacts such as layover, foreshortening and shadowing (Campbell and Wynne,

https://doi.org/10.5194/egusphere-2026-2418
Preprint. Discussion started: 12 May 2026

2011). Therefore, we analysed SRTM DEM surface elevation, aspect and slope within the study area and investigate the relationship between the terrain characteristics and the spatial distribution of detected landslides (NASA JPL, 2013). Figure 9A and B show a slight preference for slope aspects between north-east (45°) to south-west (225°). The descending SAR track travels approximately north to south, looking right towards the west/north-west, seen in Fig. A3. This results in a preferential observation geometry on the south-east facing slopes, supporting our results. Figure 9C and D show the results if we instead used the ascending track data. We expect this to show inverse results from the descending, with slight improvements in the detection between south-west and north-east. Instead, we see universally worse results from the ascending track. This is potentially due to the position of the landslides within the field of view of these images, with the landslide locations significantly offset from the SAR ascending track footprint, as seen in Fig. A3. If this is the case, the quality of results will depend on the case study being used, and users of this method should determine the optimal track for their given area of interest. The combined results (Fig. 9E and F) do not show an improvement and are unlikely to be better than either the ascending or descending in any scenario. Figure A2 does not show a strong slope influence, although this may be a more prevalent issue in areas of high relief and steep terrain like the Himalayas or Andes mountains.

This method is usable by anyone with a GEE and Google Colab profile, using datasets that are available on these platforms (Sentinel-2 multispectral and Sentinel-1 pre-processed SAR VV backscatter data). It utilises point data and is effective for events between 2015 and the present day, allowing for more than a decade of observations to be analysed. The quality of events early in the time series is likely limited, due to the Ruptures method assessing the total time series, which may put more constraints on the time frame where effective dating can occur. The only other study that improves upon ours in this respect is Fu et al. (2023), due to the use of Landsat data, which began in 1972. However, Landsat has a lower spatial resolution (30 m x 30 m), and therefore smaller landslides would be harder to detect. The highest resolution time series in Landsat would result in the 3 x 3 results from Fig. 3, showing slight smoothing from the results possible in Sentinel-2. Furthermore, the results of this study have not been compromised due to the decision to only use point data, and work in Sect 3.1 highlights that our method would not benefit from increased area analysis under the assumption that geometries are not known. Larger landslides are likely penalised within this method, as taking the residual NDVI and BSI of the point will smooth larger events if they fill the 100 m radius. However, this method must balance computationally intensity with accuracy, and aims to map all landslides within a dataset, the majority of which are small (Fig. A4).

Computationally this code is slow, due to linear looping across points. This method returns results for 100 landslides in 45-60 minutes using a 13th Gen Intel Core i7 processor with 16GB RAM. This method retrospectively dates historical landslides, and therefore a fast method is not important, however this would become more of an issue if near-real-time dating is required e.g. as part of an early-warning system. Due to the processing of calculating the residual to remove seasonality before the event, the Step 1 code generates results slowly, and to ensure code is fully encapsulated in Google Colab, faster GEE code was changed for slower alternatives within the notebook. Adaptations have been made within the code in the form of batch processing, allowing for less powerful computers to generate results more securely. This method is usable on any computer that has access to Google Colab, with lower performance computers sacrificing computing time to allow this code to still run.

https://doi.org/10.5194/egusphere-2026-2418
Preprint. Discussion started: 12 May 2026

It is important to note that the decisions made in this study were made using the dataset from Emberson et al. (2022). Potential biases from this data have therefore not been determined, and other case studies would be required to ensure that decisions like optimal SAR window length are not artifacts of this specific case study.

5.1 Limitations of this method

A landslide event occurring during a period of persistent cloud cover spanning many weeks or months could render this method unusable, due to the use of multispectral data in Step 1. This step determines the point in which the 6-months of SAR data is centred on. In scenarios where Step 1 is accurate to within 1 month, this situates the change in SAR time series in the middle of this period. However, events with prolonged cloud cover can result in a significant offset in these results. Regions that experience heavy cloud cover over long time periods (equatorial and monsoon-affected regions) will likely see a lower accuracy than those without, and if clouds persists for more than 3-months, the landslide event will likely not be captured in the 6-month window at all.

A limitation of these results, and all like them, are the inability to recognise false positive results. In examples of multi-event inventories, there is no current method of determining which 15.4% are incorrect. We generated 100 random points within the area of interest that did not overlap the landslide geometries within Emberson et al. (2022). 16% of these were dated using our method, two of which were dated overlapping the correct date window. Both correctly dated points are found within river basins, and are detecting sediment discharge as well as incomplete removal of cloud cover. This reflects similar false positive likelihoods as the real landslide dataset, and limits the reliability of conclusions drawn from analysis with these results. Similarly, many of the events are unable to be narrowed down to a window smaller than the 13-day window (7-19 March) obtained through Step 2 without sacrificing the accuracy of these results. This is due to the availability of the satellite data being used, rather than limitation within the method itself. This again can make it difficult for atmospheric analysis, as a higher temporal resolution is necessary for such conclusions. It is important to note that the reference landslide dataset is subject to the same limitation. Neither of the satellite datasets used here allows event timing to be resolved at daily precision, and the reference dataset also lacks the necessary information required for such analysis. Consequently, future studies aiming to achieve daily-scale dating would not be feasible using this dataset alone.

Applying this method to additional dataset would identify and help to remove biases from this method generated from the chosen dataset. This would also allow for further exploration into the benefits of the descending and ascending tracks. Future work to incorporate other data, and improve the robustness of this method would benefit its implementability in a wider context. Furthermore, evaluating data from contrasting regions would show how this method works in areas of varying vegetation, elevation and cloud cover. Testing this approach in a region of the Himalayas would help to assess the usability of this method in these more extreme environments. Furthermore, this would allow a wider, more complete understanding of the precision limitations, due to the current analysis using one specific event time and location.

Overall, this method is able to date landslides to a high accuracy using both Sentinel-2 multispectral data and Sentinel-1 SAR data within Google Colab. Additional work could further strengthen this method, and further constrain its reliability for use in research outside of this project.

https://doi.org/10.5194/egusphere-2026-2418
Preprint. Discussion started: 12 May 2026

6 Conclusions

This study presents a two-step methodology, implemented using the Ruptures Python package, to date landslides from pre-existing inventories. Step 1 uses optical indices from Sentinel-2 (NDVI and BSI) to provide an approximate date for a landslide event. Step 2 refines these results by examining a six-month window of Sentinel-1 SAR VV backscatter data, which also exhibits characteristic changes during landslide events.

Step 1 explores long time series effectively, but cloud cover often leads to noisy results around the expected dates. Using a landslide inventory from Zimbabwe, collected following Storm Idai on 20 March 2019, Step 1 dated 73% of events, and while only 40.0% of which fell within the expected 15–20 March window, 76.6% are dated within the month of March 2019.

Step 2 utilises SAR data to overcome the limitations of optical imagery. SAR cannot be used alone without additional dating information, as it does not experience the same consistency across long time periods. This study found that a window of ± 90 days around a landslide event was the optimal detection window for SAR backscatter data. Of the 696 points dated at this step, 84.6% are dated correctly, with an average temporal precision of 12.8 days. Combining Steps 1 and 2, 477 (68.5%) of points dated are dated correctly. Whilst we see a slight improvement in precision, with the smallest period being a single day, the average is not greatly improved (11 days), and the accuracy is worse. Therefore, it is determined that the Step 2 results are best for dating landslides, allowing for 52.8% of the dataset to be dated, of which 84.6% are dated correctly.

These results demonstrate that a combination of optical and SAR data, together with automated change point detection using Ruptures, can date landslides with high accuracy even in the absence of prior knowledge about event timing. This method reflects similar approaches in the literature, as well as improved accuracy in comparison to many SAR based methods. Such methods are beneficial in retrospectively dating inventories, increasing the availability and completeness of landslide event datasets that can be used in the study of temporal landslide triggers and controls (Guzzetti et al., 2012; Froude and Petley, 2018).

Code and data availability. The code used in this research is available at this GitHub page. https://github.com/JoannaNoyes/Dating-Landslide-Inventories-Using-Ruptures/tree/main. All satellite data used in this study is provided by the European Space Agency Copernicus program, available through Google Earth Engine. The collections used within this study are the Sentinel-2 (2015-2019) (COPERNICUS/S2), Sentinel-2 Harmonised (2020-present) (COPERNICUS/S2_SR_HARMONIZED) and Sentinel-1 C-band Synthetic Aperture Radar Ground Range Detected (COPERNICUS/S1_GRD), using VV backscatter data. The landslide data used within this study is available at Emberson et al. (2022).

https://doi.org/10.5194/egusphere-2026-2418
Preprint. Discussion started: 12 May 2026

Appendix A: Appendix A

Table A1. Sentinel satellite availability and revisit windows (the potential window between two satellite images (Claverie et al., 2018; Drusch et al., 2012)).

Dates	Available Satellites	Revisit Window (Zimbabwe)
3 April 2014 - 23 June 2015	Sentinel-1A	8-12 days
23 June 2015 - 25 April 2016	Sentinel-1A + 2A	1-10 days
25 April 2016 - March 2017	Sentinel-1A + 1B + 2A	1-3 days
March 2017 - 23 December 2021	Sentinel-1A + 1B + 2A + 2B	1-3 days
December 2021 - September 2024	Sentinel-1A + 2A + 2B (1B removed)	1-5 days
September 2024 - December 2024	Sentinel-1A + 2B + 2C (commissioning phase for 2C and 2A de-orbiting)	1-5 days
December 2024 - March 2025	Sentinel-1A + 2B + 2C + 1C (1C introduced but not effective until mid 2025)	1-5 days
March 2025 - Mid 2025	Sentinel-1A + 2B + 2C + 2A (extended) + 1C (not useable)	1-3 days
Mid 2025	Sentinel-1A + 1C + 2B + 2C + 2A (extended)	1-3 days

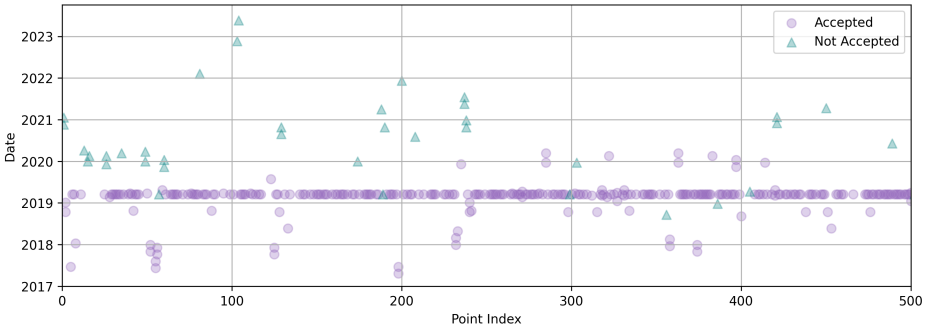

Figure A1. Dates of 500 points from this dataset coloured depending on the mean change between the time series before and after that date. Purple points indicate physically plausible changes (negative NDVI, positive BSI), teal triangle points indicate implausible changes (positive NDVI and/or negative BSI). Teal triangle points are removed in the end product of this report.

Author contributions. J.N., S.P. and G.B designed the research. J.N. implemented the code, analysed the data, and wrote the text. All authors helped to interpret the results and commented on the draft of the manuscript.

https://doi.org/10.5194/egusphere-2026-2418
Preprint. Discussion started: 12 May 2026

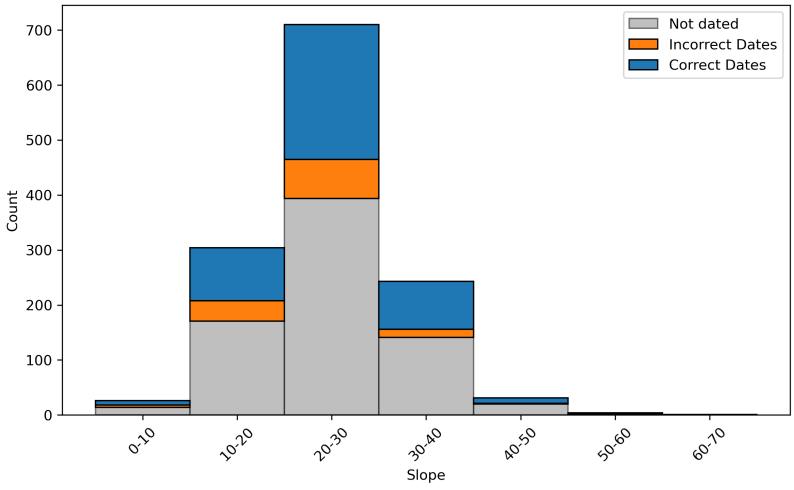

Figure A2. Slope of each landslide, showing the landslides that were note dated (grey), were dated incorrectly (orange) and correctly (blue)

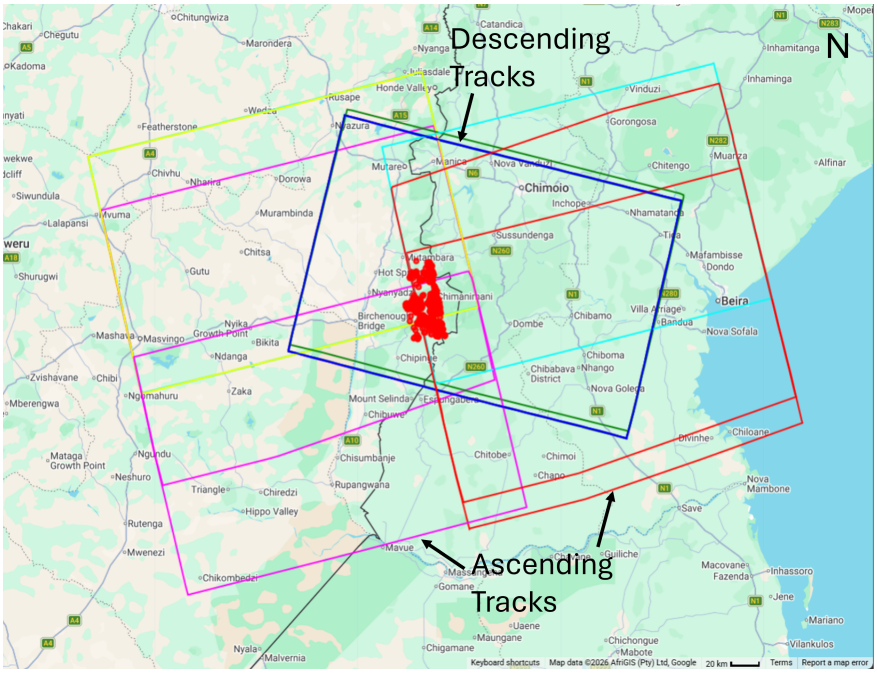

Figure A3. Footprint of all the Sentinel-1 SAR images between 2019-02-20 and 2019-04-05 that overlap the area of interest. The landslide data is shown as red points. Generated in GEE. Six descending tracks, eight ascending tracks. Basemap: ©Google, ©AfriGIS (Pty) Ltd.

https://doi.org/10.5194/egusphere-2026-2418
Preprint. Discussion started: 12 May 2026

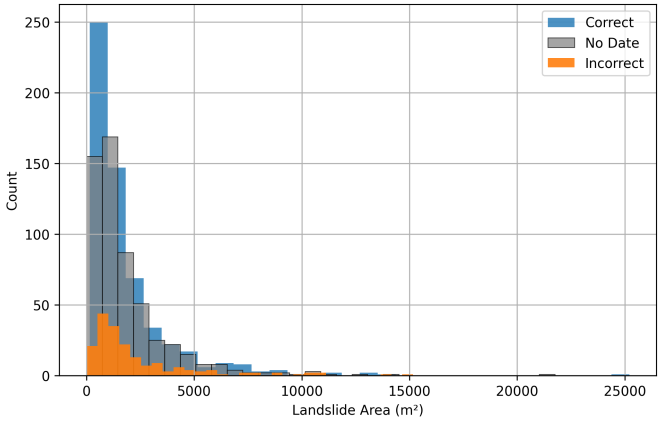

Figure A4. Histogram of the size distributions for the correctly (blue), incorrectly (orange) and not dated (grey) landslides within the inventory.

Competing interests. The authors declare that they have no conflict of interest.

375 *Acknowledgements.* The authors are grateful for early discussions and advice given by Dave Milledge, which led to improvements in the approach used. In particular, we appreciate access to the ALDI code, and discussions about methodological design.

https://doi.org/10.5194/egusphere-2026-2418
Preprint. Discussion started: 12 May 2026

References

Barbera, L., Maltese, A., and Conoscenti, C.: Automated Dating of Recent Landslides Using Sentinel-2 and Sentinel-1 on Google Earth Engine, Remote Sensing, 17, 3270, https://doi.org/https://doi.org/10.3390/rs17193270, 2025.

Baum, R. L. and Godt, J. W.: Early Warning of rainfall-induced Shallow Landslides and Debris Flows in the USA, Landslides, 7, 259–272, https://doi.org/https://doi.org/10.1007/s10346-009-0177-0, 2009.

Bostjančić, I., Filipović, M., Gulam, V., and Markotić, I.: Landslide inventory for Pannonian Croatia, Mendeley Data, V1, https://doi.org/10.17632/9rss4pgvzc.1, accessed: 2026-03-12, 2025.

British Geological Survey: National Landslide Database, https://www.bgs.ac.uk/geology-projects/landslides/national-landslide-database/, accessed: 2026-03-12, 2023.

Burrows, K., Marc, O., and Remy, D.: Using Sentinel-1 Radar Amplitude Time Series to Constrain the Timings of Individual landslides: a Step Towards Understanding the Controls on monsoon-triggered Landsliding, Natural Hazards and Earth System Sciences, 22, 2637–2653, https://doi.org/https://doi.org/10.5194/nhess-22-2637-2022, 2022.

Burrows, K., Milledge, D. G., and Ferrario, M. F.: Detection of Landslide timing, Reactivation and Precursory Motion during the 2018, Lombok, Indonesia Earthquake Sequence with Sentinel-1, Earth Surface Dynamics, 13, 1039–1057, https://doi.org/https://doi.org/10.5194/esurf-13-1039-2025, 2025.

Campbell, J. B. and Wynne, R. H.: Introduction to Remote Sensing, Fifth Edition, Guilford Press, ISBN 9781609181772, 2011.

Claverie, M., Ju, J., Masek, J. G., Dungan, J. L., Vermote, E. F., Roger, J., Shakun, S. V., and Justice, C.: The Harmonized Landsat and Sentinel-2 Surface Reflectance Data Set, Remote Sensing of Environment, 219, 145–161, https://doi.org/https://doi.org/10.1016/j.rse.2018.09.002, 2018.

Deijns, A., Dewitte, O., Thiery, W., d'Oreye, N., Malet, J.-P., and Kervyn, F.: Timing Landslide and Flash Flood Events from SAR satellite: a Regionally Applicable Methodology Illustrated in African cloud-covered Tropical Environments, Natural Hazards and Earth System Sciences, 22, 3679–3700, https://doi.org/https://doi.org/10.5194/nhess-22-3679-2022, 2022.

Delforge, D., Wathelet, V., Below, R., Lanfredi Sofia, C., Tonnelier, M., van Loenhout, J. A. F., and Speybroeck, N.: EM-DAT: the Emergency Events Database, International Journal of Disaster Risk Reduction, 124, 105 509, https://doi.org/https://doi.org/10.1016/j.ijdrr.2025.105509, 2025.

Drusch, M., Del Bello, U., Carlier, S., Colin, O., Fernandez, V., Gascon, F., Hoersch, B., Isola, C., Laberinti, P., Martimort, P., Meygret, A., Spoto, F., Sy, O., Marchese, F., and Bargellini, P.: Sentinel-2: ESA's Optical High-Resolution Mission for GMES Operational Services, Remote Sensing of Environment, 120, 25–36, https://doi.org/https://doi.org/10.1016/j.rse.2011.11.026, 2012.

Emberson, R., Kirschbaum, D. B., Amatya, P., Tanyas, H., and Marc, O.: Insights from the Topographic Characteristics of a Large Global Catalog of rainfall-induced Landslide Event Inventories, Natural Hazards and Earth System Sciences, 22, 1129–1149, https://doi.org/https://doi.org/10.5194/nhess-22-1129-2022, 2022.

Endo, T.: Probable Distribution of the Amount of Rainfall Causing Landslides, Annual Report 1968, Sapporo, 1969.

Froude, M. J. and Petley, D. N.: Global Fatal Landslide Occurrence from 2004 to 2016, Natural Hazards and Earth System Sciences, 18, 2161–2181, https://doi.org/https://doi.org/10.5194/nhess-18-2161-2018, 2018.

Fu, S., de Jong, S., Deijns, A., Geertsema, M., and de Haas, T.: The SWADE Model for Landslide Dating in Time Series of Optical Satellite Imagery, Landslides, 20, 913–932, https://doi.org/https://doi.org/10.1007/s10346-022-02012-4, 2023.

https://doi.org/10.5194/egusphere-2026-2418
Preprint. Discussion started: 12 May 2026

Fu, S., de Jong, S., Hou, X., de Vries, J., Deijns, A., and de Haas, T.: A Landslide Dating Framework Using a Combination of Sentinel-1 SAR and -2 Optical Imagery, Engineering Geology, 329, 107 388, https://doi.org/https://doi.org/10.1016/j.enggeo.2023.107388, 2024.

Geological Survey of India: Compiled Landslide Inventory, https://bhukosh.gsi.gov.in/Bhukosh/Public, 2024.

Guzzetti, F., Mondini, A. C., Cardinali, M., Fiorucci, F., Santangelo, M., and Chang, K.: Landslide Inventory maps: New Tools for an Old Problem, Earth-Science Reviews, 112, 42–66, https://doi.org/https://doi.org/10.1016/j.earscirev.2012.02.001, 2012.

Haque, U., da Silva, P. F., Devoli, G., Pilz, J., Zhao, B., Khaloua, A., Wilopo, W., Andersen, P., Lu, P., Lee, J., Yamamoto, T., Keellings, D., Wu, J., and Glass, G. E.: The human cost of global warming: Deadly landslides and their triggers (1995–2014), Science of the Total Environment, 682, 673–684, https://doi.org/https://doi.org/10.1016/j.scitotenv.2019.03.415, 2019.

Jaafari, A.: An Overview of Triggering and Causing Factors of Landslides, Disaster Risk Reduction, p. 25–45, https://doi.org/https://doi.org/10.1007/978-981-97-4680-4_2, 2024.

Juang, C. S., Stanley, T. A., and Kirschbaum, D. B.: Using Citizen Science to Expand the Global Map of landslides: Introducing the Cooperative Open Online Landslide Repository (COOLR), PLOS ONE, 14, e0218 657, https://doi.org/https://doi.org/10.1371/journal.pone.0218657, 2019.

Kirschbaum, D. B., Adler, R., Hong, Y., Hill, S., and Lerner-Lam, A.: A Global Landslide Catalog for Hazard applications: method, results, and Limitations, Natural Hazards, 52, 561–575, https://doi.org/https://doi.org/10.1007/s11069-009-9401-4, 2009.

Knapp, K. R., Kruk, M. C., Levinson, D. H., Diamond, H. J., and Neumann, C. J.: The International Best Track Archive for Climate Stewardship (IBTrACS), Bulletin of the American Meteorological Society, 91, 363–376, https://doi.org/10.1175/2009bams2755.1, 2010.

Korchagina, I. A., Goleva, O. G., Savchenko, Y. Y., and Bozhikov, T. S.: The Use of Geographic Information Systems for Forest Monitoring, Journal of physics. Conference Series, 1515, 032 077–032 077, https://doi.org/https://doi.org/10.1088/1742-6596/1515/3/032077, 2020.

Malamud, B. D., Turcotte, D. L., Guzzetti, F., and Reichenbach, P.: Landslide Inventories and Their Statistical Properties, Earth Surface Processes and Landforms, 29, 687–711, https://doi.org/https://doi.org/10.1002/esp.1064, 2004.

Milledge, D. G., Bellugi, D. G., Watt, J., and Densmore, A. L.: Automated Determination of Landslide Locations after Large Trigger events: Advantages and Disadvantages Compared to Manual Mapping, Natural Hazards and Earth System Sciences, 22, 481–508, https://doi.org/https://doi.org/10.5194/nhess-22-481-2022, 2022.

NASA JPL: NASA Shuttle Radar Topography Mission Global 1 arc second, https://doi.org/10.5067/MEASURES/SRTM/SRTMGL1.003, nASA Land Processes Distributed Active Archive Center, 2013.

Pennington, C. V. L., Bossu, R., Ofli, F., Imran, M., Qazi, U., Roch, J., and Banks, V. J.: A near-real-time Global Landslide Incident Reporting Tool Demonstrator Using Social Media and Artificial Intelligence, International Journal of Disaster Risk Reduction, 77, 103 089, https://doi.org/https://doi.org/10.1016/j.ijdrr.2022.103089, 2022.

Petley, D.: Global Patterns of Loss of Life from Landslides, Geology, 40, 927–930, https://doi.org/https://doi.org/10.1130/g33217.1, 2012.

Segoni, S., Piciullo, L., and Gariano, S. L.: A Review of the Recent Literature on Rainfall Thresholds for Landslide Occurrence, Landslides, 15, 1483–1501, https://doi.org/https://doi.org/10.1007/s10346-018-0966-4, 2018.

Singh, R., Pal, M., and Biswas, M.: Cloud Detection Methods for Optical Satellite Imagery: a Comprehensive Review, Geomatics, 5, 27–27, https://doi.org/https://doi.org/10.3390/geomatics5030027, 2025.

Truong, C., Oudre, L., and Vayatis, N.: Selective Review of Offline Change Point Detection Methods, Signal Processing, 167, 107 299, https://doi.org/https://doi.org/10.1016/j.sigpro.2019.107299, 2020.

https://doi.org/10.5194/egusphere-2026-2418
Preprint. Discussion started: 12 May 2026

Wang, W., Motagh, M., Xia, Z., Plank, S., Li, Z., Orynbaikyzy, A., Zhou, C., and Roessner, S.: A Framework for Automated Landslide Dating Utilizing SAR-Derived Parameters Time-Series, an Enhanced Transformer Model, and Dynamic Thresholding, International Journal of Applied Earth Observation and Geoinformation, 129, 103 795–103 795, https://doi.org/https://doi.org/10.1016/j.jag.2024.103795, 2024.

Wen, T. H. and Teo, T. A.: Landslide Inventory Mapping from LANDSAT-8 NDVI Time Series Using Adaptive Landslide Interval Detection, ISPRS Annals of the Photogrammetry, Remote Sensing and Spatial Information Sciences, V-3-2022, 557–562, https://doi.org/https://doi.org/10.5194/isprs-annals-v-3-2022-557-2022, 2022.

Woodhouse, I. H.: Introduction to Microwave Remote Sensing, CRC Press, ISBN 9781315272573, https://doi.org/https://doi.org/10.1201/9781315272573, 2017.

Yuniawan, R. A., Rifa'i, A., Faris, F., Subiyantoro, A., Satyaningsih, R., Hidayah, A. N., Hidayat, R., Mushthofa, A., Ridwan, B. W., Priangga, E., Muntohar, A. S., Jetten, V. G., Westen, C. J. c., Bout, B. V. d., and Sutanto, S. J.: Revised Rainfall Threshold in the Indonesian Landslide Early Warning System, Geosciences, 12, 129, https://doi.org/https://doi.org/10.3390/geosciences12030129, 2022.

Zhong, C., Liu, Y., Gao, P., Chen, W., Li, H., Hou, Y., Nuremanguli, T., and Ma, H.: Landslide Mapping with Remote sensing: Challenges and Opportunities, International Journal of Remote Sensing, 41, 1555–1581, https://doi.org/https://doi.org/10.1080/01431161.2019.1672904, 2019.